HHS Public Access

Author manuscript

Brain Struct Funct. Author manuscript; available in PMC 2022 February 22.

Published in final edited form as:

Brain Struct Funct. 2015 January ; 220(1): 457–468. doi:10.1007/s00429-013-0667-7.

Enhanced characterization of the zebrafish brain as revealed by super resolution track-density imaging

Jeremy F.P. Ullmann[a,b,*], **Fernando Calamante**[c,d], **Shaun P. Collin**[b,e], **David C. Reutens**[a], **Nyoman D. Kurniawan**[a]

[a]Centre for Advanced Imaging, The University of Queensland, Brisbane 4072, Queensland, Australia

[b]School of Biomedical Sciences, The University of Queensland, Brisbane 4072, Queensland, Australia.

[c]Florey Institute of Neuroscience and Mental Health, Melbourne 3084, Victoria, Australia.

[d]Department of Medicine, Austin Health and Northern Health, University of Melbourne, Melbourne 3084, Victoria, Australia.

[e]School of Animal Biology and the UWA Oceans Institute, The University of Western Australia, Perth 6000, Western Australia, Australia.

Abstract

In this study we explored the use of super-resolution track density imaging (TDI) for neuroanatomical characterization of the adult zebrafish brain. We compared the quality of image contrast and resolution obtained with T_2* magnetic resonance imaging (MRI), diffusion tensor based imaging (DTI), TDI, and histology. The anatomical structures visualized in 5 μm TDI maps corresponded with histology. Moreover the super-resolution property and the local-directional information provided by directionally-encoded color TDI facilitated delineation of a larger number of brain regions, commissures and small white matter tracks when compared to conventional MRI and DTI. In total, we were able to visualize 17 structures that were previously unidentifiable using MR microimaging, such as the four layers of the optic tectum. This study demonstrates the use of TDI for characterization of the adult zebrafish brain as a pivotal tool for future phenotypic examination of transgenic models of neurological diseases.

Keywords

zebrafish; brain; magnetic resonance; diffusion-weighted imaging; track-density imaging; probabilistic tractography

[*]**Corresponding Author:** Centre for Advanced Imaging, The University of Queensland, Brisbane 4072, QLD, Australia. Telephone: +61 7 3346 0363, Fax: +61 7 3346 0330, j.ullmann@uq.edu.au.

Introduction

Zebrafish are an established experimental model for the investigation of neurodegenerative disorders. Large clutch sizes, transparent larval stages, and the ability to perform forward or reverse genetic analyses have particularly facilitated the use of embryonic and larval zebrafish (Lieschke and Currie 2007). Mature zebrafish, which possess well-developed endocrine, sensory, and motor systems (Bally-Cuif and Vernier 2010), a range of complex behaviours such as social interactions (Saverino and Gerlai 2008), learning and memory (Gomez-Laplaza and Gerlai 2010; Norton and Bally-Cuif 2010; Al-Imari and Gerlai 2008) and a physiology similar to mammals (Bally-Cuif and Vernier 2010), have been recognized as beneficial to investigations of neurological diseases (Alfaro et al. 2011; Siebel et al. 2011; Wong et al. 2010; Keller and Murtha 2004; Mathur and Guo 2010; Ramirez et al. 2012; Haud et al. 2011; Williams et al. 2011). As adult zebrafish continue to be used as an experimental model, new techniques are being developed to better characterize their behaviour (Cachat et al. 2011), neuronal activity (Pineda et al. 2011), neurochemistry (Kabli et al. 2009) and neuromorphology (Rao et al. 2009; Ullmann et al. 2010b; Ullmann et al. 2010a; Kabli et al. 2006).

Magnetic resonance imaging (MRI) is an important technique for investigating the morphology, connectivity, and function of the brain. Although initially developed for imaging humans, MRI has become a key platform for imaging small animals and is now routinely performed on mice (Richards et al. 2011; Ullmann et al. 2012), rats (Petiet et al. 2007), and zebrafish (Ullmann et al. 2010b; Kabli et al. 2009; Ullmann et al. 2010a). However, MRI becomes increasingly challenging as the size of the animal decreases. To delineate ever-smaller brain regions, higher resolution and contrast are required. Tradeoffs between image acquisition parameters must carefully be considered to accommodate these requirements. For example, the adult zebrafish brain has a relatively small size ($5mm^3$), with a volume approximately 64 times smaller than that of an adult mouse brain. Consequently, an increase of at least four times image resolution in each plane is necessary to resolve the zebrafish brain microstructures. This, however, would result in a reduction in the signal to noise ratio by a factor of eight. In this case, ultra-high resolution imaging is undertaken on fixed brains to enable longer scan times and an increased number of averages.

A new method called track density imaging (TDI) has recently been developed, which offers both high resolution and novel contrast (Calamante et al. 2010) that cannot be obtained with conventional MRI sequences. During post-processing, TDI incorporates data from whole-brain fiber tracking to yield image maps at a higher resolution than the acquired data, *i.e.* it achieves super-resolution (Calamante et al. 2011). These TDI maps can also encode information on fiber directionality, which can be displayed in directionally-encoded colour (DEC) (Calamante et al. 2010). In particular, the technique of DEC short-tracks TDI (DEC stTDI) is a modified variant specifically designed to provide high contrast fiber-direction information, while avoiding intensity saturation from dense white matter structures (Calamante et al. 2012b). The high resolution and high contrast properties of these maps make this technique ideal for the study of the fine structures in the zebrafish brain. In this paper, we therefore explore the use of super-resolution track density imaging (TDI) as a

contrast mechanism for enhanced characterization of the zebrafish brain, and demonstrate its potential role in phenotypic examination of animal models of neurodegenerative disorders.

Materials and Methods

Sample Preparation

All animal experiments were performed according to procedures approved by the University of Queensland Animal Ethics Committee (AEC No SBMS/074/08). Four adult wildtype zebrafish (AB strain) were euthanized with an overdose of tricaine methane sulfonate (MS222, 1:10,000 in water). The dorsal cranium was removed from the fish and the head was immersion fixed and stained in a solution of 4% paraformaldehyde in PBS and 0.5% Magnevist (Bayer) for 12 hours. The brain and ventral cranium, were mounted onto a small piece of plastic, and then placed in a 5 mm NMR tube and filled with Fomblin (perfluoropolyether, Ausimont, Morristown, NJ, USA) for imaging. The hydrophobic nature of Fomblin, an inert perfluoropolyether oil solution, prevents leaching of Magnevist out from the sample to the medium.

MR Data Acquisition

Diffusion-weighted magnetic resonance images were acquired using a Bruker (Ettlingen, Germnay) 16.4 Tesla vertical magnet with a bore diameter of 89 mm, a Bruker micro 2.5 imaging gradient, and a custom-made horizontal 5 × 4 mm solenoid radiofrequency (rf) coil. Sample temperature was maintained at 22°C using a circulating water gradient cooling system. Three-dimensional diffusion-weighted spin-echo images were acquired with the following parameters: TR/TE 450/21.83 ms, FOV 6.9 × 2.6 × 2.6 mm^3, acquisition matrix 144 × 54 × 54, NEX 4, resulting in an isotropic resolution of 48 μm. Each dataset was composed of two low diffusion weighted images (b= 0 s/mm^2) and thirty high diffusion weighted (b=5000 s/mm^2) images with encoding gradient (δ/Δ = 2.5/14 ms) vectors uniformly distributed using an electrostatic approach (Jones et al. 1999). Total imaging time was 46 hours and 40 minutes. The 3D data set was symmetrically zero-filled to 288 × 108 × 108 matrix resulting in an isotropic resolution of 24 μm.

For each sample, two high-resolution anatomical scans were also acquired with a 3D FLASH (Frahm et al. 1986) gradient echo T_2*-weighted image sequence. The first scan had a 48 μm isotropic image resolution and the following imaging parameters: TR/TE = 50/8.3 ms; matrix 128 × 54 × 54; NEX = 16, and 39 min imaging time; while the second scan was obtained at a 10 μm isotropic resolution TR/TE = 50/8.3 ms; matrix 592 × 260 × 260; NEX = 16, and a 15 hour imaging time.

Super-resolution TDI Map Reconstruction

To correct for possible drift during the long scan time, a 3D rigid body 3-parameter model registration with correlation ratio cost function was performed using the first b0 image in each dataset as a template using the program FSL FLIRT 4.1.9 (http://fsl.fmrib.ox.ac.uk/fsl/fsl-4.1.9). Fiber-tracks were then generated using the program MRtrix 0.2.9 (brain.org.au/software/mrtrix) (Tournier et al. 2012), which uses constrained spherical deconvolution (CSD) to resolve crossing-fibers by estimating the fiber orientation distribution (FOD) at

each voxel (Tournier et al. 2007). Probabilistic fiber-tracking (Behrens et al., 2003) was performed using the iFOD1 algorithm (Tournier et al. 2010), with 0.024 mm step-size, maximum angle between steps = 45°, *lmax* = 6. Fiber-tracks were terminated when they exited the brain or when the FOD < 0.02. A whole brain CSD probabilistic-tractography dataset of 60 million short fiber tracks was calculated, with a minimum track length of 2-voxel size and a maximum length of 10 voxel size (Calamante et al. 2012b). This whole-brain tractography dataset was then used to generate DEC stTDI maps, using a 5 μm isotropic (super-resolution) voxel size. In these maps, the colour in each voxel is determined by averaging the colours of all track segments contained within the voxel. Therefore, the colour-coding indicates the local fiber orientation (red: rostral-caudal, green: medial-lateral, blue: dorsal-ventral).

For the purpose of comparison, the same diffusion weighted imaging (DWI) data set was also analysed using the diffusion tensor model (Basser 1995), and the results displayed as DEC fractional anisotropy (FA) maps (Pajevic and Pierpaoli 1999). These maps have the same resolution as the acquired DWI data, and the colour encodes the direction of the principal eigenvector of the diffusion tensor.

Bootstrap method was not performed to test the general stTDI map reproducibility due to high demand on computational resources. To calculate the mean and deviations of stTDI map dispersion values using bootstrap method (e.g. as described in Jeurissen et al., 2011), this would require at least 50 repetitions of 60 million streamlines of stTDI runs or generation of 3billion streamlines. Instead, to characterise in more detail the CNR behaviour with increasing number of tracks and how this affect visualisation of structures in the zebrafish brain, stTDI maps were generated using 1, 5, 10, 20, 40 and 60 millions tracks. Excellent brain structure identification, contrast and colour saturation were observed in stTDI generated using > 20 million tracks. 60 million stTDI for all dataset was chosen at the end to ensure superior reproduction of stTDI maps (see Supplementary Fig. 1). Each stTDI calculation was completed in 6 hours using 6-core Xeon workstation using 70 GB RAM.

Targeted Probabilistic Fiber-Tracking of White Matter Structures

Due to the rich contrast present in the DEC stTDI maps, they can be used to delineate the extent of white matter structures. Specific regions of interest (ROIs) were identified and then combined with target ROIs to assess structural connectivity using targeted tractography (Mori and van Zijl 2002). Approximately 5,000 streamlines were generated from each seed ROI using similar probabilistic fiber-tracking parameters as above, except that full-length streamlines (in contrast to short tracks) were generated to visualise the extent of the structural connection. In particular, targeted tractography was carried out for seed ROIs located in the forebrain and midbrain.

Histology

Upon completion of diffusion and anatomical scans two scanned brains were dissected from their respective craniums and embedded in Paraplast Plus tissue embedding medium (Oxford Labware), sectioned at 10 μm, stained with luxol fast blue for myelin and

counterstained with cresyl violet for neurons. Briefly, the sections were deparaffinised in xylene, rehydrated in ethanol and water and then incubated in a 1% luxol fast blue stain for 4 hours. Subsequently the sections differentiated in 0.05% Lithium carbonate and 70% ethanol solutions. Slides were then incubated in a 0.25% cresyl violet solution for 3 min before dehydrating, clearing, and mounting. Histological sections closest to the TDI slices were visually identified and digitally scanned for comparison using a Zeiss Axio Imager Z2 microscope fitted with a motorised stage and a Metafer Slide Scanning Platform (MetaSytems, Germany). A Zeiss 20× 0.8NA PlanApochromatic objective and Metasystems CoolCube camera were used for image acquisition. All images were processed using Adobe Photoshop CS5 and figures compiled with Adobe Illustrator CS5.

Results

Figure 1 demonstrates the results of whole-brain DEC stTDI processing at 5μm resolution produced from 48μm 30-directions HARDI data acquired at 16.4T for one of the brain samples studied; similar results were obtained for the other samples (data not shown). Directionally encoded color (DEC) stTDI maps enable exceptional visualization of fine white matter tracks, characterizing not only the spatial extent of numerous brain structures, but also fiber directionality.

Figure 2 shows a comparison of T_2*-weighted images, DEC FAmaps, and DEC-stTDI maps of a series of slices through the zebrafish brain. While T_2* images are of high-resolution ($10\mu m^3$), limited contrast between tissue types, particularly noticeable in the telencephalon (Fig. 2a,b), restricts detailed delineation of substructures. In the DEC FA maps contrast is enhanced by local directional information but low-resolution impedes detailed visualization. In contrast, the high resolution and high contrast in DEC-stTDI maps results in vastly improved definition of fiber tracks, cellular layers and nuclei.

Figures 3 and 4 demonstrate the anatomical consistency between super-resolution track density imaging and conventional histology of the zebrafish brain. Three selected regions were shown at higher magnification, through the telencephalon and optic tectum with corresponding histological sections at approximately the same position. In Figure 3 numerous structural subdivisions could be visualized based upon color changes in the directionally encoded color TDI maps. In our maps, the color green indicates a medial-lateral fiber orientation, red to a rostral-caudal fiber orientation, and blue a dorsal-ventral fiber orientation. Color variations indicate fiber tracks with orientations in between the major directions listed above. In Figure 3a,b the subdivisions of the dorsal telencephalon (D) can be delineated as follows: the medial zone (Dm) appears bright yellow, the ventral surface of the dorsal zone (Dd) appears green, the lateral zone (Dl) appears bright pink at the surface and dark more medially, the posterior zone (Dp) characterized by the hyperintense white color; and the remaining central area the central zone (Dc). In the ventral telencephalon, the anterior part of the parvicellular preoptic nucleus (PPa) can also be identified as bright pink region. DEC stTDI also enabled characterization of numerous fiber tracks and commissures, such as the lateral forebrain bundle (LFB), which is visible in blue as it projects dorso-ventrally through Dc to the level of the anterior commissure, where it then extends caudally into the diencephalon (Fig. 3a,b); the anterior commissure which

can be distinguished as it divides into its dorsal (CantD) and ventral (CantV) components (Fig. 1c,d); and the caudal end of the medial olfactory tract (MOT), which is shown in red, lateral to dorsal anterior commissure (Fig. 3c,d).

A similar correspondence is also found when examining the optic tectum. DEC *st*TDI maps clearly reveal nuclei, white matter tracks and commissures including the nucleus of the medial longitudinal fascicle (nMLF, Fig 4a,b), the oculomotor nerves (III, Fig 4a,b), the fiber-tracks that make up the commissura ansulata (Cans, Fig 4a, b), and the tractus tectobulbaris (TTB, Fig 4c,d). The distinct lamination pattern of the teleost optic tectum can also be visualized with DEC *st*TDI. The findings from DEC *st*TDI maps are consistent with previous studies (Kishida 1979; Laufer and Vanegas 1974; Corbo et al. 2012) which have shown the optic tectum to contain four primary cellular layers, the superficial grey and white zone (SWGZ), the central zone (CZ), the deep white zone (DWZ) and the periventricular grey zone (PGZ) (Northcutt 1983)

Figure 5 demonstrates the enhanced ability to identify neuroanatomical structures in the zebrafish brain. Many of these structures could not be delineated in the MRI-based zebrafish brain atlas (Ullmann et al. 2010b). In particular, a greater number of fiber tracks and commissures could be delineated and a complete list can be found in Table 1. TDI also facilitated the visualization of a number of additional brain regions not visible on T_2* imaging, including the caudal lobe of the cerebellum (LCa), caudal octavolateralis nucleus (CON), and the different cellular layers in the olfactory bulb.

Figure 6 shows the result of *targeted* tractography that was generated from specific seeding regions of interest (ROIs) identified on the DEC *st*TDI maps. The following white matter fiber-track profiles were generated: (1) The medial (Fig 6e) and lateral (Fig 6c) olfactory tracts, which are shown in red/pink and yellow/orange, respectively. (2) The dorsal and ventral anterior commissures, which are shown in blue and green, respectively (Fig. 6b). (3) The oculomotor nerve which is shown in pastel green and pink (Fig. 6g). (4) The crossed tecto-bulbar tract shown in purple (Fig. 6g). Fiber tracking throughout the brain confirms established zebrafish neuroanatomy. Fig 6. visualizes nicely the medial olfactory tract coursing more ventrally than the lateral olfactory tract and the oculomotor nerves projecting from between the tectum and hypothalamus dorsally to the oculmotor nerve that is located below the tectal ventricle.

Discussion

This study demonstrates the role of super-resolution track density imaging (*st*TDI) for high contrast whole-brain imaging and for guiding target probabilistic tractography to reveal specific white matter structures in the adult zebrafish. We compared DEC *st*TDI maps with conventional T_2* images, diffusion tensor based images (DEC FA), and histological sections to demonstrate the efficacy of DEC *st*TDI maps for neuroanatomical characterization of the zebrafish brain. The structures visualized in the DEC *st*TDI maps were consistent with our histological analysis, supporting the veracity of the anatomical contrast in these maps, which is in agreement with previous TDI studies in the mouse (Calamante et al. 2012b) and human (Calamante et al. 2012a) brains. Moreover the super-resolution property and

the local-directional information provided by DEC stTDI, combined with the high signal to noise ratio provided by ultra-high MRI at 16.4T, enabled enhanced examination of the zebrafish brain.

Detailed descriptions of adult zebrafish brain anatomy and connections have already been established with histology (Wullimann et al. 1996; Rink and Wullimann 2004; Mueller et al. 2011) and conventional MRI (Ullmann et al. 2010b), yet both methods possess shortcomings, which limit their use. In conventional histology, a large library of markers exists facilitating the identification of many neuroanatomical structures. However, the low resolution along the slice orientation and the difficulty of obtaining a perfect series of sections in a single brain limits whole brain analyses (Yang et al. 2012). MRI lacks a library of cellular markers but permits acquisition of isotropic images at a lower resolution than microscopy. As a result, researchers rely on a variety of pulse sequences to exploit variations in either proton density and tissue relaxation properties (Johnson et al. 2010; McLaren et al. 2009; Johnson et al. 2012), and/or a limited number of contrast agents. To date the majority of studies have utilized gadolinium-based contrast agents, such as Magnevist® and Pro-Hance®, however Manganese, a functional contrast agent (Koretsky and Silva 2004) (Leergaard et al. 2003), and more recently potassium dichromate (Rowland 2011; Zhang et al. 2010) and myelin-specific (Frullano et al. 2012) contrast agents have also been used.

In contrast to T_1/T_2* MRI sequences, TDI is based on the information contained in a whole-brain tractogram generated from DWI data, and therefore relies on the innate structure and connectivity of the tissue to provide contrast. Furthermore, the super-resolution properties of the TDI technique (Calamante et al. 2011) provide a major boost to the spatial resolution achievable by this MRI method. In this study, we were able to delineate a greater number of structures using DEC *st*TDI than when compared to T_2* maps. For example, the clear visualization of the anterior commissure facilitated the demarcation of a border between the dorsal telencephalon and the ventral telencephalon (Fig. 5a), which corroborates previous immunohistochemical and molecular results (Mueller et al. 2011; Ganz et al. 2012). Similarly, some fiber tracks such as the lateral and medial forebrain bundles (LFB and MFB), which are very small in diameter (45μm) and therefore only appear as faint lines in the 10μm T_2*-weighted image and as coarse red pixels in the 48μm DEC FA maps, could clearly be distinguished as discrete fiber bundles in the 5μm DEC *st*TDI maps. As a result, DEC *st*TDI, with its very high spatial resolution and the high anatomical contrast provided by the orientation information, enabled us to delineate 30 fiber bundles, including commissures, fiber tracks and nerves. Table 1 lists all of the tracts, commissures and nerves that were successfully identified, which includes 17 structures that were previously unidentifiable using MR histology.

The very high resolution and contrast achievable using DEC *st*TDI maps could play an important role in creating more detailed multi-modal brain atlases. Previous studies have demonstrated the utility of DEC *st*TDI for visualization of small brain structures, such as the thalamic nuclei (Calamante et al. 2012a), the cerebellar peduncles (Calamante et al. 2010), and other structures in the human brain (Cho et al. 2013). By registering the TDI data to other MR images and histology, more detailed high-resolution atlases could be created, due to the complementary information of all these imaging modalities.

DEC *st*TDI can also assist in creating more detailed connectivity maps. The enhanced resolution facilitates the placement of very small regions of interest enabling more specific targeted tractography. These improvements would be particularly useful for brains such as the zebrafish, which have a volume over 100 times smaller than the human brain. In this study, we found this to be the case for the targeted tractography analyses we performed as tractography results confirm previous retrograde and anterograde labeling experiments (von Bartheld et al. 1984; Rink and Wullimann 2004; Wullimann et al. 1996).

While this study and previous studies have found that DEC *st*TDI maps replicate histological data, these comparisons have been limited to qualitative analyses because of the different contrast mechanisms. For example, our histological sections demonstrate the location of neurons and fiber tracts but do not contain directional information. However, a new tractography technique, three-dimensional polarized light imaging (3D-PLI) has been recently developed that can visualize the orientation of nerve fibers based upon their birefringence (Axer et al. 2011; Palm et al. 2010). Birefringence, is the product of the arrangement of proteins and lipids in myelin, and has an optical anisotropy that reflects the spatial fiber architecture of nerve fibers. By carefully collecting a series of sections and calculating fiber orientation maps, whole brain fiber tracking can be performed and compared with DWI data. Furthermore, as birefringence data is collected from histological data, the acquired resolution is very high with voxel sizes as small as $100\mu m^3$ in the human brain (Palm et al. 2010). This voxel size is directly comparable to that achieved in human TDI data (Calamante et al. 2010), and could potentially be used to validate the DEC *st*TDI technique. However, it should be noted that 3D-PLI has a number of technical difficulties when used for whole-brain fiber-tracking, including accurate registration of the large number of PLI sections into a 3D volume, vector reorientation, and partial volume effects in voxels containing more than one fiber population (akin to the limitations of the diffusion tensor model).

The quality of DEC stTDI is dependent, among other factors (see references Calamante et al. 2010 and Calamante et al. 2012b for a more detailed discussion), on the spatial resolution and angular resolution of the acquired DWI data. This is necessary to obtain a reliable fiber orientation distribution (FOD) for modeling of fiber crossing, which in turn has a direct influence on the quality of whole-brain tractography. For examining the zebrafish brain with a volume of only $(3mm)^3$ and containing substructures that are in the order of 10–50μm in diameter, imaging with a high spatial resolution is paramount. Three-dimensional gradient echo (3D GE) MRI sequences at ultra-high field strength are capable of acquiring 10μm isotropic resolution images but a large number of scan averages (NEX=16) are necessary to achieve a good signal to noise ratio (SNR). While it is possible to acquire a data with a longer scan time, this will mostly contribute to an increase SNR rather than additional tissue contrast. Theoretically, to obtain 3D GE image at 5 μm isotropic resolution and maintaining SNR level as in the 10μm images, NEX needs to be increased by 2^3, which is increasing the scan time from 15h to 120h (considerable time cost). In contrast, the combination of such spatial resolution and number of scans is not practical for HARDI acquisition. For example, it took 55h to collect 48μm isotropic resolution data with 30 diffusion directions, 2 b0 images and 4 NEX at 16.4T in the current study. For reducing the DWI scan to 15h, we would have only been able to collect data with 6 diffusion encoding directions and

2b0, which is suitable for DTI processing only. Therefore, super-resolution 5um DEC stTDI provides additional value by enabling nuclei and fiber-tracks not previously seen in the 3D GE image to be visualised at even higher spatial resolution, although at the expense of longer acquisition times than those required for standard DTI.

It should be noted that TDI contrast is the reverse of that in a GE image. In general, myelinated white matter tracks appear hyperintense in TDI, hypointense in GE, and blue after luxol fast blue staining. This could make comparisons confusing and potentially misleading. More importantly, hypointense areas in TDI maps do not necessarily represent nuclei but could instead represent areas with a low number of streamlines. For example, throughout the telencephalon there are numerous hypointense areas, such as in the medial zone of the dorsal telencephalon (see sagittal section in Fig. 1) or the dorsolateral zone in the dorsal telencephalon (Dl in Fig. 3a). As seen in histological sections, these areas do not correspond to large nuclei but to areas with a reduced number of fibers.

Conclusion

This study demonstrates super-resolution TDI provides enhanced characterization of the zebrafish brain. DEC *st*TDI maps corresponded to those provided using histology, and allowed delineation of a greater number of brain regions, commissures, and fiber tracks when compared to T_2* imaging. With the increased use of transgenic adult zebrafish for examination of neurological diseases, we expect this methodology to be an important additional imaging tool for phenotypic examination.

Supplementary Material

Refer to Web version on PubMed Central for supplementary material.

Acknowledgement

We are grateful to the National Health and Medical Research Council (NHMRC) of Australia, and the Australian Research Council (ARC LE100100074 and FT110100726) for their support. We would also like to thank the National Imaging Facility (NIF) and the Queensland NMR Network (QNN) for access to the 16.4T scanner and technical support. The Florey Institute of Neuroscience and Mental Health is supported by Victorian State Government infrastructure funds. We would also like to thank Jane Ellis for assistance with the histology.

Abbreviations:

3D GE	Three-dimensional gradient echo
3D-PLI	Three-dimensional polarized light imaging
AC	Anterior cerebellar tract
Cans	Ansulate commissure
CantD	Anterior commissure, dorsal part
CantV	Anterior commissure, ventral part
CC	Cerebellar crest

CCeG	Cerebellar corpus, granular layer
CCeM	Cerebellar corpus, molecular layer
Ccer	Cerebellar commissure
CON	Caudal octavolateralis nucleus
Cpop	Postoptic commissure
Cpost	Posterior commissure
CSD	Constrained spherical deconvolution
Cven	Ventral rhombencephalic commissure
CZ	Central zone of the optic tectum
D	Dorsal telencephalon
Dc	Central zone of the dorsal telencephalon
Dd	Dorsal zone of the dorsal telencephalon
DEC	Directionally encoded color
Dl	Lateral zone of the dorsal telencephalon
Dm	Medial zone of the dorsal telencephalon
DOT	Dorsomedial optic tract
Dp	Posterior zone of the dorsal telencephalon
DTI	Diffusion tensor imaging
DWI	Diffusion weighted imaging
DWZ	Deep white zone of the optic tectum
FA	Fractional anisotropy
FOD	Fiber orientation distribution
FOV	Field of view
FR	Habenula-interpeduncular tract
GL	Glomerular layer
HARDI	High angular-resolution diffusion-weighted imaging
III	Oculomotor nerve
IO	Inferior olive
LCa	Caudal lobe of the cerebellum

LFB	Lateral forebrain bundle
LLF	Lateral longitudinal fascicle
LOT	Lateral olfactory tract
LVII	Facial lobe
LX	Vagal lobe
MA	Mauthner axon
MFB	Medial forebrain bundle
MLF	Medial longitudinal fascicle
MOT	Medial olfactory tract
MRI	Magnetic resonance imaging
NEX	Number of averages
NIN	Interpeduncular nucleus
nMLF	Nucleus of the medial longitudinal fascicle
OlfN	Olfactory nerve
ON	Optic nerve
PGZ	Periventricular grey zone of the optic tectum
POF	Primary olfactory layer
PPa	Parvocellular preoptic nucleus
RF	Radio frequency
SNR	Signal to noise ratio
SWGZ	Superficial grey and white zone of the optic tectum
TDI	Track density imaging
TE	Echo time
TeO	Optic tectum
TL	Longitudinal torus
TMCA	Anterior mesencephalon-cerebellar tract
TPM	Pretecto-mammillary tract
TR	Repetition time
TTB	Tractus tectobulbaris

TTBc	Crossed tecto-bulbar tract
Val	Lateral division of the valvula cerebelli
Vas	Vascular lacuna of area postrema

References

Al-Imari L, Gerlai R (2008) Sight of conspecifics as reward in associative learning in zebrafish (Danio rerio). Behav Brain Res 189:216–219. [PubMed: 18243353]

Alfaro JM, Ripoll-Gomez J, Burgos JS (2011) Kainate administered to adult zebrafish causes seizures similar to those in rodent models. European Journal of Neuroscience 33 (7):1252–1255.

Axer M, Amunts K, Grassel D, Palm C, Dammers J, Axer H, Pietrzyk U, Zilles K (2011) A novel approach to the human connectome: ultra-high resolution mapping of fiber tracts in the brain. NeuroImage 54 (2):1091–1101. [PubMed: 20832489]

Bally-Cuif L, Vernier P (2010) Organization and physiology of the zebrafsih nervous system. In: Zebrafish, vol 29. Fish Physiology. Elsevier Inc.,

Basser PJ (1995) Inferring microstructural features and the physiological state of tissues from diffusion-weighted images. NMR Biomed 8 (7–8):333–344. [PubMed: 8739270]

Best JD, Alderton WK (2008) Zebrafish: An *in vivo* model for the study of neurological diseases. Neuropsychiatric Disease and Treatment 4 (3):567–576. [PubMed: 18830398]

Cachat J, Stewart A, Utterback E, Hart P, Gaikwad S, Wong K, Kyzar E, Wu N, Kalueff AV (2011) Three-dimensional neurophenotyping of adult zebrafish behavior. Plos One 6 (3):e17597. [PubMed: 21408171]

Calamante F, Tournier J-D, Jackson GD, Connelly A (2010) Track-density imaging (TDI): super-resolution white matter imaging using whole-brain track-density mapping. NeuroImage 53 (4):1233–1243. [PubMed: 20643215]

Calamante F, Tournier JD, Heidemann RM, Anwander A, Jackson GD, Connelly A (2011) Track density imaging (TDI): Validation of super resolution property. Neuroimage 56 (3):1259–1266. [PubMed: 21354314]

Calamante F, Oh SH, Tournier JD, Park SY, Son YD, Chung JY, Chi JG, Jackson GD, Park CW, Kim YB, Connelly A, Cho ZH (2012a) Super-resolution track-density imaging of thalamic substructures: Comparison with high-resolution anatomical magnetic resonance imaging at 7.0T. Hum Brain Mapp.

Calamante F, Tournier JD, Kurniawan ND, Yang Z, Gyengesi E, Galloway GJ, Reutens DC, Connelly A (2012b) Super-resolution track-density imaging studies of mouse brain: Comparison to histology. NeuroImage 59 (1):286–296. [PubMed: 21777683]

Cho ZH, Calamante F, Chi JG (2013) 7.0 Tesla MRI Brain White Matter Atlas In. Panmun Co, Ltd, Seoul, South Korea,

Corbo CP, Othman NA, Gutkin MC, Alonso Adel C, Fulop ZL (2012) Use of different morphological techniques to analyze the cellular composition of the adult zebrafish optic tectum. Microsc Res Techniq 75 (3):325–333.

Frahm J, Haase A, Matthaei D (1986) Rapid three-dimensional MR imaging using the FLASH technique. Journal of Comp Assist Tomography 10 (2):363–368.

Frullano L, Zhu J, Wang C, Wu C, Miller RH, Wang Y (2012) Myelin imaging compound (MIC) enhanced magnetic resonance imaging of myelination. J Med Chem 55 (1):94–105. [PubMed: 22098543]

Ganz J, Kaslin J, Freudenreich D, Machate A, Geffarth M, Brand M (2012) Subdivisions of the adult zebrafish subpallium by molecular marker analysis. J Comp Neurol 520 (3):633–655. [PubMed: 21858823]

Gomez-Laplaza LM, Gerlai R (2010) Latent learning in zebrafish (Danio rerio). Behav Brain Res 208 (2):509–515. [PubMed: 20043955]

Haud N, Kara F, Diekmann S, Henneke M, Willer JR, Hillwig MS, Gregg RG, Macintosh GC, Gartner J, Alia A, Hurlstone AF (2011) rnaset2 mutant zebrafish model familial cystic

leukoencephalopathy and reveal a role for RNase T2 in degrading ribosomal RNA. Proc Natl Acad Sci U S A 108 (3):1099–1103. [PubMed: 21199949]

Johnson GA, Badea A, Brandenburg J, Cofer G, Fubara B, Liu S, Nissanov J (2010) Waxholm space: An image-based reference for coordinating mouse brain research. NeuroImage 53 (2):365–372. [PubMed: 20600960]

Johnson GA, Calabrese E, Badea A, Paxinos G, Watson C (2012) A multidimensional magnetic resonance histology atlas of the Wistar rat brain. NeuroImage 62 (3):1848–1856. [PubMed: 22634863]

Jones DK, Simmons A, Williams SCR, Horsfield MA (1999) Non-invasive assessment of axonal fiber connectivity in the human brain via diffusion tensor MRI. Magnetic Resonance in Medicine 42 (1):37–41. [PubMed: 10398948]

Kabli S, Alia A, Spaink HP, Verbeek FJ, de Groot HJM (2006) Magnetic resonance microscopy of adult zebrafish. Zebrafish 3 (4):431–439. [PubMed: 18377223]

Kabli S, Spaink HP, De Groot HJM, Alia A (2009) In vivo metabolite profile of adult zebrafish brain obtained by high-resolution localized magnetic resonance spectroscopy. Journal of Magnetic Resonance Imaging 29 (2):275–281. [PubMed: 19161175]

Keller ET, Murtha JM (2004) The use of mature zebrafish (*Danio rerio*) as a model for human aging and disease. Comparative Biochemistry and Physiology, Part C 138:335–341. [PubMed: 15533791]

Kishida R (1979) Comparative study on the teleostean optic tectum. Lamination and cytoarthitecture. Journal fur Hirnforschung 20:57–67. [PubMed: 479577]

Koretsky AP, Silva AC (2004) Manganese-enhanced magnetic resonance imaging (MEMRI). NMR Biomed 17 (8):527–531. [PubMed: 15617051]

Laufer M, Vanegas H (1974) The optic tectum of a perciform teleost. II. Fine structure. J Comp Neurol 154:61–96. [PubMed: 4815184]

Leergaard TB, Bjaalie JG, Devor A, Wald LL, Dale AM (2003) In vivo tracing of major rat brain pathways using manganese-enhanced magnetic resonance imaging and three-dimensional digital atlasing. NeuroImage 20 (3):1591–1600. [PubMed: 14642470]

Lieschke GJ, Currie PD (2007) Animal models of human disease: zebrafish swim into view. Nature Reviews 8:353–367.

Mathur P, Guo S (2010) Use of zebrafish as a model to understand mechanisms of addiction and complex neurobehavioral phenotypes. Neurobiol Dis 40 (1):66–72. [PubMed: 20493262]

McLaren DG, Kosmatka KJ, Oakes TR, Kroenke CD, Kohama SG, Matochik JA, Ingram DK, Johnson SC (2009) A population-average MRI-based atlas collection of the rhesus macaque. NeuroImage 45 (1):52–59. [PubMed: 19059346]

Mori S, van Zijl PC (2002) Fiber tracking: principles and strategies - a technical review. NMR Biomed 15 (7–8):468–480. [PubMed: 12489096]

Mori S, Zhang J (2006) Principles of diffusion tensor imaging and its applications to basic neuroscience research. Neuron 51 (5):527–539. [PubMed: 16950152]

Mueller T, Dong ZQ, Berberoglu MA, Guo S (2011) The dorsal pallium in zebrafish, Danio rerio (Cyprinidae, Teleostei). Brain Res 1381:95–105. [PubMed: 21219890]

Northcutt RG (1983) Evolution of the optic tectum in ray-finned fishes. In: Davis RE, Northcutt RG (eds) Fish Neurobiology, Vol 2. Higher brain areas and functions, vol 2. University of Michigan Press, Ann Arbor, pp 1–42

Norton W, Bally-Cuif L (2010) Adult zebrafish as a model organism for behavioural genetics. BMC Neuroscience 11 (1):90. [PubMed: 20678210]

Pajevic S, Pierpaoli C (1999) Color schemes to represent the orientation of anisotropic tissues from diffusion tensor data: application to white matter fiber tract mapping in the human brain. Magn Reson Med 42 (3):526–540. [PubMed: 10467297]

Palm C, Axer M, Grassel D, Dammers J, Lindemeyer J, Zilles K, Pietrzyk U, Amunts K (2010) Towards ultra-high resolution fibre tract mapping of the human brain - registration of polarised light images and reorientation of fibre vectors. Front Hum Neurosci 4:9. [PubMed: 20461231]

Petiet A, Hedlund L, Johnson GA (2007) Staining methods for magnetic resonance microscopy of the rat fetus. Journal of Magnetic Resonance Imaging 25:1192–1198. [PubMed: 17520739]

Pineda R, Beattie CE, Hall CW (2011) Recording the adult zebrafish cerebral field potential during pentylenetetrazole seizures. J Neurosci Meth 200 (1):20–28.

Ramirez IB, Pietka G, Jones DR, Divecha N, Alia A, Baraban SC, Hurlstone AF, Lowe M (2012) Impaired neural development in a zebrafish model for Lowe syndrome. Hum Mol Genet 21 (8):1744–1759. [PubMed: 22210625]

Rao KD, Alex A, Verma Y, Thampi S, Gupta PK (2009) Real-time *in vivo* imaging of adult zebrafish brain using optical coherence tomography. Journal of Biophotonics:1–4.

Richards K, Watson C, Buckley RF, Kurniawan ND, Yang Z, Keller MD, Beare R, Bartlett PF, Egan GF, Galloway GJ, Paxinos G, Petrou S, Reutens DC (2011) Segmentation of the mouse hippocampal formation in magnetic resonance images. NeuroImage 58 (3):732–740. [PubMed: 21704710]

Rink E, Wullimann MF (2004) Connections of the ventral telencephalon (subpallium) in the zebrafish (Danio rerio). Brain Res 1011 (2):206–220. [PubMed: 15157807]

Rowland IJ (2011) Dichromate as a Stain for Mr Microscopy. I S Biomed Imaging:742–745.

Saverino C, Gerlai R (2008) The social zebrafish: behavioral responses to conspecific, heterospecific, and computer animated fish. Behav Brain Res 191:77–87. [PubMed: 18423643]

Siebel AM, Piato AL, Capiotti KM, Seibt KJ, Bogo MR, Bonan CD (2011) PTZ-induced seizures inhibit adenosine deamination in adult zebrafish brain membranes. Brain Res Bull 86 (5–6):385–389. [PubMed: 21907764]

Tournier JD, Calamante F, Connelly A (2007) Robust determination of the fibre orientation distribution in diffusion MRI: non-negativity constrained super-resolved spherical deconvolution. NeuroImage 35 (4):1459–1472. [PubMed: 17379540]

Tournier JD, Calamante F, Connelly A Improved probabilistic streamlines tractography by 2nd order integration over fibre orientation distributions. In: International Society for Magnetic Resonance in Medicine, Stockholm, Sweden, 2010. p 1670

Tournier JD, Calamante F, Connelly A (2012) MRtrix: Diffusion tractography in crossing fiber regions. Int J Imag Syst Tech 22 (1):53–66.

Ullmann JF, Keller MD, Watson C, Janke AL, Kurniawan ND, Yang Z, Richards K, Paxinos G, Egan GF, Petrou S, Bartlett P, Galloway GJ, Reutens DC (2012) Segmentation of the C57BL/6J mouse cerebellum in magnetic resonance images. NeuroImage 62 (3):1408–1414. [PubMed: 22658976]

Ullmann JFP, Cowin G, Kurniawan ND, Collin SP (2010a) Magnetic resonance histology of the adult zebrafish brain: optimization of fixation and gadolinium contrast enhancement. NMR Biomed 23 (4):341–346. [PubMed: 19950106]

Ullmann JFP, Cowin G, Kurniawan ND, Collin SP (2010b) A three-dimensional digital atlas of the zebrafish brain NeuroImage 51 (1):76–82. [PubMed: 20139016]

von Bartheld CS, Meyer DL, Fiebig E, Ebbesson SOE (1984) Central connections of the olfactory bulb in the goldfish, *Carassius auratus*. Cell and Tissue Research 238 (3):475–487. [PubMed: 6084554]

Williams LR, Wong K, Stewart A, Suciu C, Gaikwad S, Wu N, Dileo J, Grossman L, Cachat J, Hart P, Kalueff AV (2011) Behavioral and physiological effects of RDX on adult zebrafish. Comp Biochem Physiol C Toxicol Pharmacol.

Wong K, Stewart A, Gilder T, Wu N, Frank K, Gaikwad S, Suciu C, DiLeo J, Utterback E, Chang K, Grossman L, Cachat J, Kalueff AV (2010) Modeling seizure-related behavioral and endocrine phenotypes in adult zebrafish. Brain Res 1348:209–215. [PubMed: 20547142]

Wullimann MF, Rupp B, Reichert H (1996) Neuroanatomy of the zebrafish brain: a topological atlas. Birkhäuser Verlag, Basel

Yang Z, Richards K, Kurniawan ND, Petrou S, Reutens DC (2012) MRI-guided volume reconstruction of mouse brain from histological sections. J Neurosci Meth 211 (2):210–217.

Zhang X, Bearer EL, Perles-Barbacaru AT, Jacobs RE (2010) Increased anatomical detail by in vitro MR microscopy with a modified Golgi impregnation method. Magn Reson Med 63 (5):1391–1397. [PubMed: 20432310]

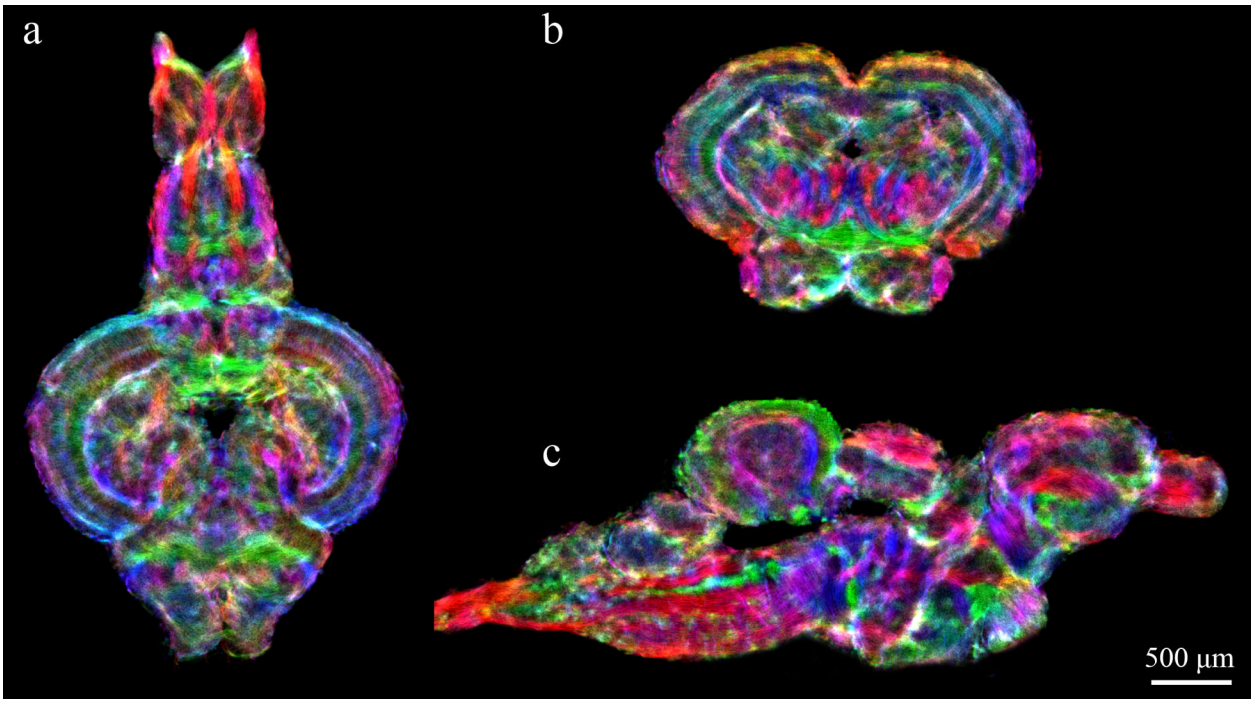

Figure 1:
Sample DEC stTDI maps (5μm isotropic resolution) calculated from whole-brain fiber-tracking results, which were generated from DWI data acquired on a 16.4T scanner (at 48μm isotropic resolution). Horizontal section (a), axial section (b), and sagittal section (c) of whole brain fiber-tracking results. Color-coding indicates the local fiber orientation (with red: rostral-caudal, green: medial-lateral, and blue: dorsal-ventral.

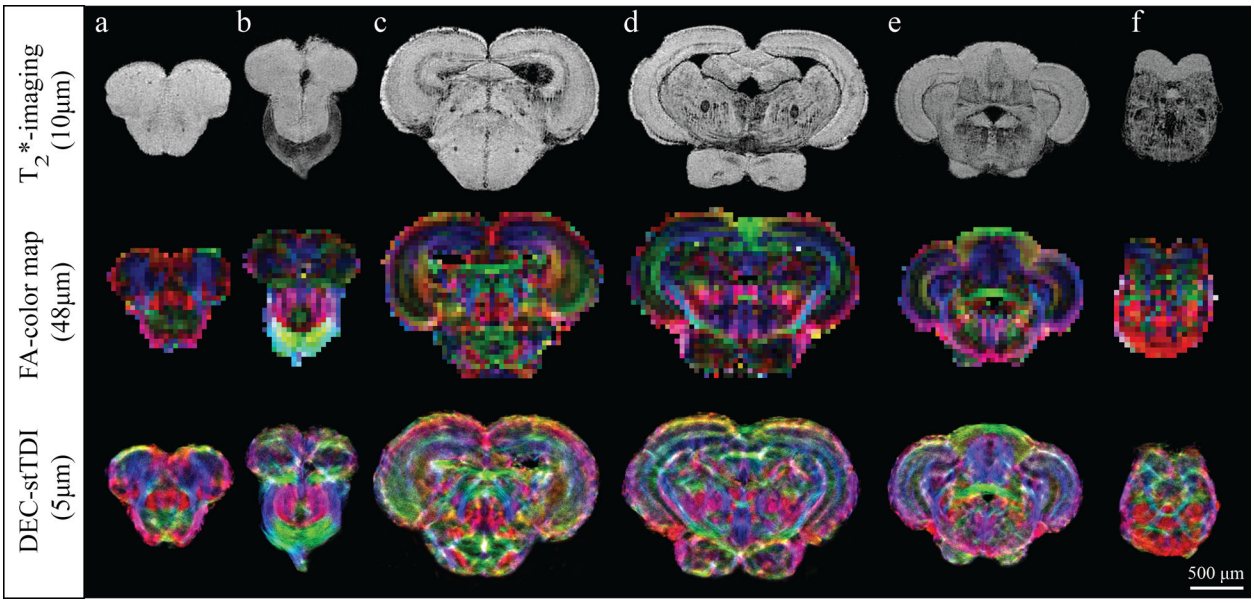

Figure 2:

Comparison of T_2*-weighted images, DEC FA maps, and DEC-stTDI maps in six different axial slices of the zebrafish brain. Top row: T_2*-images with a 10μm isotropic resolution. Middle row: corresponding DEC FA maps with a 48μm isotropic resolution. Bottom row: corresponding super-resolution DEC-*st*TDI maps with 5μm isotropic resolution. DEC-*st*TDI maps were generated from the original 48μm HARDI using a 5μm super-resolution grid and 60 million tracks. The color-coding indicates the primary local orientation (red: rostral-caudal, green: medial-lateral, blue: dorsal-ventral).

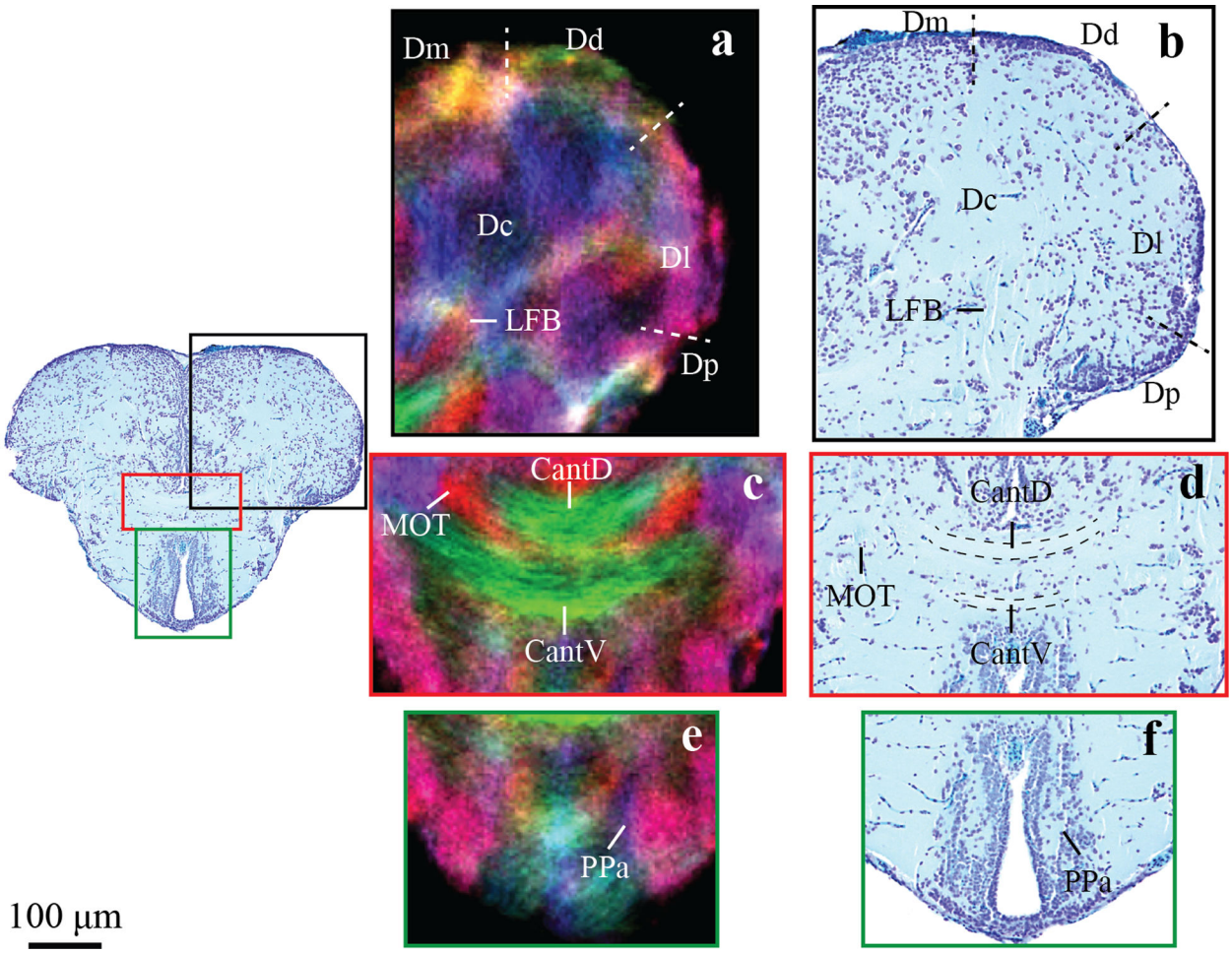

Figure 3:

Zoomed in regions of an axial image through the telencephalon in DEC stTDI maps (a,c,e) and histological sections (b,d,f). Identified structures include the dorsal anterior commissure, CantD; ventral anterior commissure, CantV; central zone of the dorsal telencephalon, Dc; dorsal zone of the dorsal telencephalon, Dd; lateral zone of the dorsal telencephalon, Dl; medial zone of the dorsal telencephalon, Dm; posterior zone of the dorsal telencephalon, Dp; lateral forebrain bundle, LFB; anterior part of the parvocellular preoptic nucleus, PPa. The DEC stTDI maps have 5µm isotropic resolution, and the color-coding indicates the local orientation (red: rostral-caudal, green: medial-lateral, blue: dorsal-ventral).

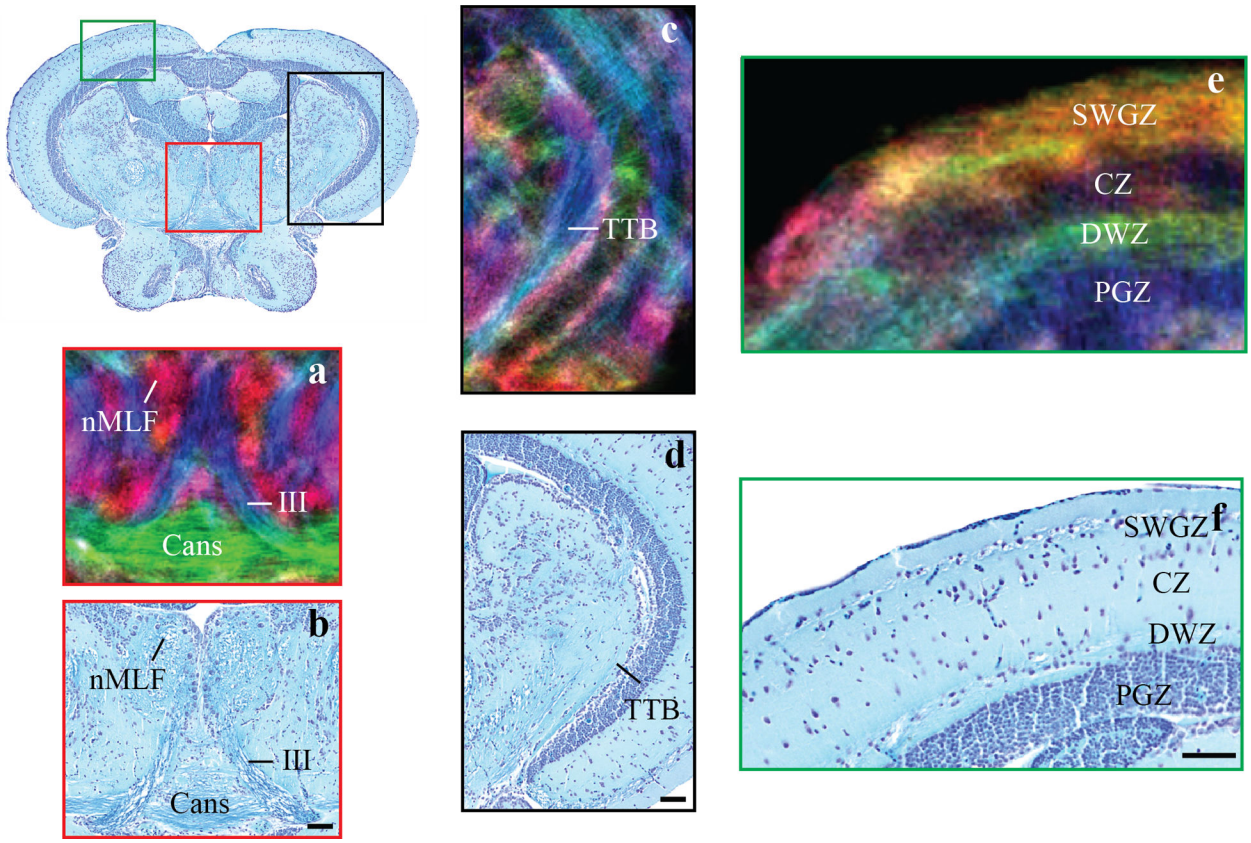

Figure 4:

Zoomed in regions of an axial image through the mesencephalon in DEC stTDI maps (a, c, e) and histological sections (b,d,f). Identified structures include: the oculomotor nerves, III; the commissura ansulata, Cans; the central zone of the optic tectum, CZ; the deep white zone of the optic tectum, DWZ, the nucleus of the medial longitudinal fascicle, nMLF; the periventricular grey zone of the optic tectum, PGZ; and the superficial grey and white zone of the optic tectum, SWGZ. The DEC stTDI maps have 5μm isotropic resolution, and the color-coding indicates the local orientation (red: rostral-caudal, green: medial-lateral, blue: dorsal-ventral).

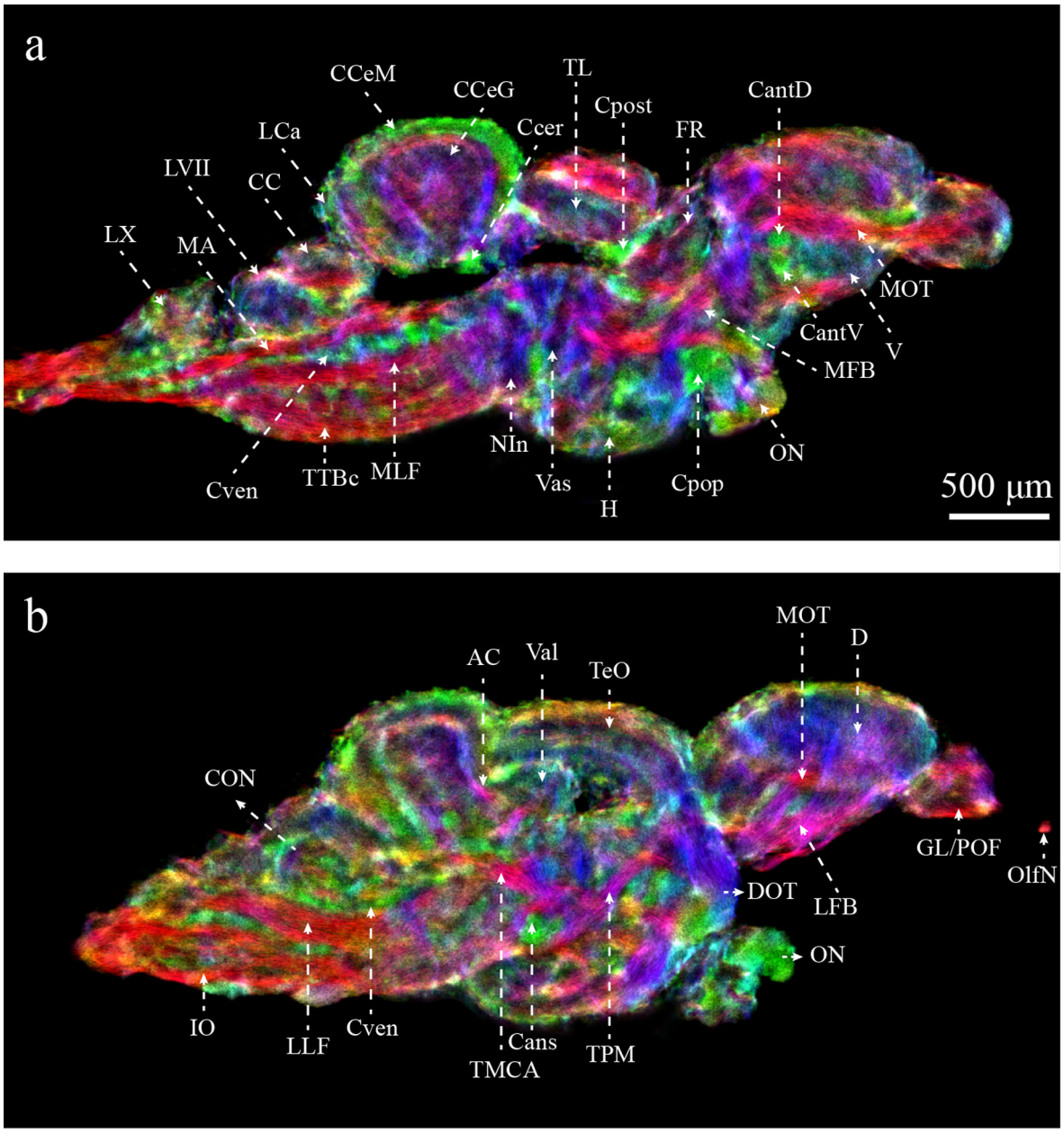

Figure 5:

Enhanced characterization of the zebrafish brain from DEC-stTDI images (5µm isotropic resolution). Identified structures include: AC, anterior cerebellar tract; Cans, ansulate commissure; CantD, anterior commissure, dorsal part; CantV, anterior commissure, ventral part; CC, cerebellar crest; CCeG, cerebellar corpus, granular layer; CCeM, cerebellar corpus, molecular layer; Ccer, cerebellar commissure; CON, caudal octavolateralis nucleus; Cpop, postoptic commissure; Cpost, posterior commissure; Cven, ventral rhombencephalic commissure; DOT, dorsomedial optic tract; FR, habenula-interpeduncular tract; GL/POF, glomerular/primary olfactory layers; IO, inferior olive; LCa, caudal lobe of the cerebellum; LFB, lateral forebrain bundle; LLF, lateral longitudinal fascicle; LVII, facial lobe; LX, vagal lobe; MA, Mauthner axon; MFB, medial forebrain bundle; MLF, medial longitudinal

fascicle; MOT, medial olfactory tract; NIn, interpeduncular nucleus; OlfN, olfactory nerve; ON, optic nerve; TeO, optic tectum; TL, longitudinal torus; TMCA, anterior mesencephalon-cerebellar tract; TPM, pretecto-mammillary tract; TTBc, crossed tecto-bulbar tract; Val, lateral division of the valvula cerebelli; Vas, vascular lacuna of area postrema. Color-coding indicates the local orientation (red: rostral-caudal, green: medial-lateral, blue: dorsal-ventral).

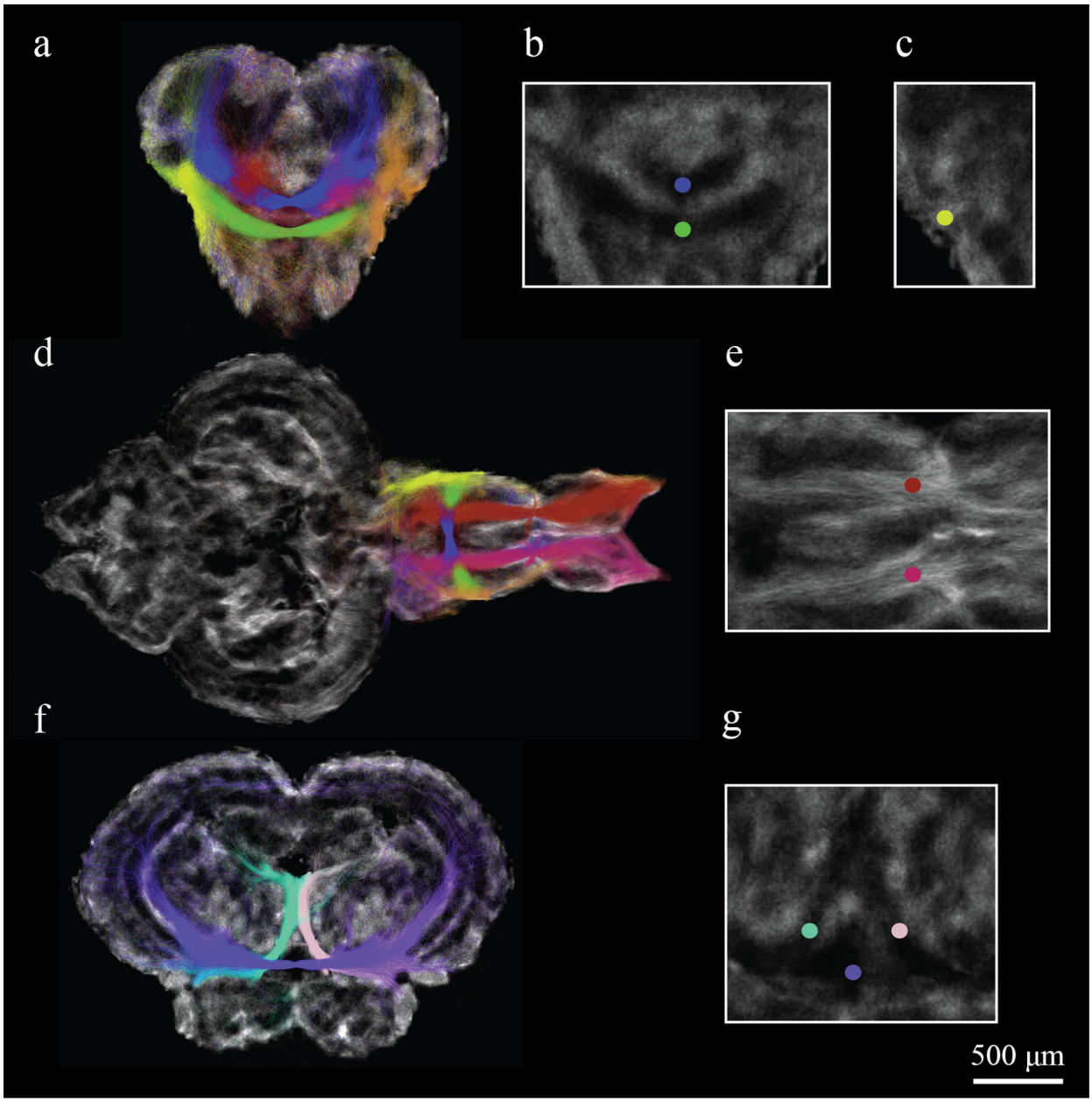

Figure 6:

Targeted tractography for seeds defined in the forebrain and midbrain of the zebrafish brain. Seed ROIs and fiber tracks are labeled with different colors including: (a-e) red/pink for the medial and lateral olfactory tracts, blue/green for the dorsal and ventral anterior commissure; (f, g) pastel green/pink for the oculomotor nerves and purple for the crossed tecto-bulbar tract. Fiber tracking illustrates nicely the connections that the olfactory tracts make between the olfactory bulbs and the ventral telencephalon with a few connections projecting into the diencephalon.

Table 1.

List of fiber tracks visible with DEC *sf*TDI.

Commissures	Fiber Tracts	Nerves
Ansulate commissure	Medial olfactory tract	Oculomotor nerve
Dorsal anterior commissure *	Lateral forebrain bundle *	Trochlear nerve *
Ventral anterior commissure *	Medial forebrain bundle *	Octaval nerve *
Habenular commissure	Pretecto-mammillary tract	Anterior lateral line *
Horizontal commissure *	Lateral longitudinal fascicle	Posterior lateral line *
Posterior commissure *	Medial longitudinal fascicle	
Optic chiasma	Crossed tecto-bulbar tract *	
Supraoptic commissure *	Uncrossed tecto-bulbar tract	
Secondary gustatory commissure *	Anterior mesencephalo-cerebellar tract	
Ventral rhombencephalic commissure *	Anterior cerebellar tract *	
	Posterior cerebellar tract	
	Secondary gustatory tract	
	Inferior olive *	
	Optic tract	
	Mauthner axon *	

* Indicates fiber tracts previously unidentifiable with magnetic resonance histology.